Adsorption of RB-5 Dyestuff onto Boric Acid-Zinc Nanoalloys: Isotherm, Kinetic, and Thermodynamic Investigations

[1]Hasan İLHAN, [2]Ömer GULER, [3]Tuncay ŞİMŞEK, [4]Salih ALKAN*
[1]*Ankara University, Institute of Biotechnology, Department of Biotechnology, Ankara, TURKEY.*
[2]*Munzur University, Rare Earth Elements Application and Research Center, Tunceli, TURKEY.*
[3]*Department of Mechanical and Metal Technologies, Kırıkkale University, Kirikkale, TURKEY.*
[4]*Department of Chemistry, Faculty of Arts and Sciences Ordu University, Ordu, TURKEY.*
salihalkan@odu.edu.tr*

(Received on 28th March 2025, accepted in revised form 8th September 2025)

Abstract: In this study, boric acid-zinc (BA-Zn) nanoalloys were employed as an adsorbent for the removal of RB-5 dyestuff from aqueous solutions. The investigation focused on analyzing the impact of the initial dyestuff concentration, solution pH, temperature, and equilibrium contact time on the adsorption process of RB-5. The adsorption behavior of RB-5 onto the surface of BA-Zn-nanoalloys was explored, with a particular emphasis on the influence of initial dyestuff concentration and solution pH. The adsorption equilibrium data were subjected to analysis using Langmuir, Freundlich, DRK, and Temkin isotherm models. The results revealed a consistent alignment of RB-5 adsorption with both Langmuir and Temkin isotherms. Notably, the Langmuir adsorption capacity of BA-Zn-nanoparticles for RB-5 adsorption was determined to be 11.77 mg/g at a temperature of 25°C. In the Temkin isotherm model, an adsorption constant (AT) of 1.003 was obtained. The calculated adsorption energy from the DR adsorption model was 1.09 kJ/mol, implying a physical interaction-driven adsorption process. The empirical data further exhibited conformity with the pseudo-second order kinetic model, reflecting the rate-limiting step and overall kinetics of the adsorption process. Complementary to this, thermodynamic parameters such as enthalpy (ΔH^0), Gibbs free energy (ΔG^0), and entropy (ΔS^0) were evaluated to discern the energetics of BA-Zn-nanoparticle RB-5 adsorption. This study not only underscores the effectiveness of BA-Zn nanoalloys as a potential adsorbent for RB-5 dyestuff removal but also contributes to the understanding of the underlying adsorption mechanisms and energetics. The insights gained hold implications for the development of sustainable and efficient strategies for wastewater treatment and environmental protection.

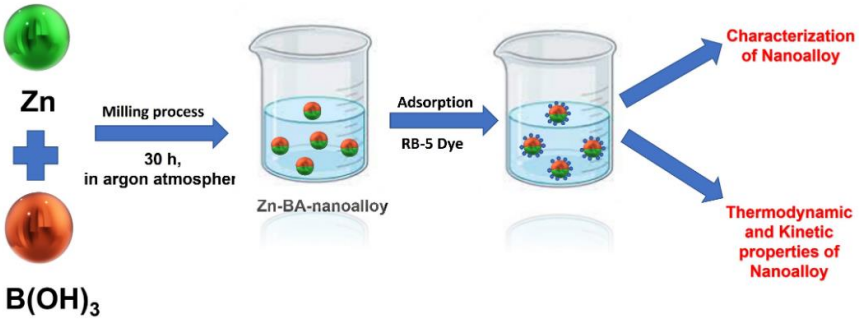

Keywords: Nanocrystals, Ball milling, Boric acid, Zinc, RB-5.

Introduction

Reactive Black 5 (RB5) is widely used in the apparel industries, such as cotton, wool, nylon, and synthetics [1]. However, reducing RB5's azo group produces toxic, carcinogenic, and mutagenic aromatic amines [2]. The dye's structural complexity leads to chemical stability, persistence, and non-biodegradability [3]. RB5's resistance to change in acidity, alkalinity, heat, light, and its high solubility pose challenges in wastewater treatment [4]. Hence, the need arises for cost-effective yet potent water treatment approaches to eliminate RB5 from wastewater streams. Presently, diverse methods are explored for RB5 removal, encompassing chemical coagulation [5], anion exchange [6], adsorption [7] and biodegradability [8]. Adsorption stands out as a versatile and appealing technique worldwide. It offers simplicity, affordability, and effectiveness in dye removal from wastewater. Among them, commercial activated carbon is highly effective [9]. Yet, its cost hampers wider use. Thus, researchers explore alternatives: clay, zeolites, chitosan, siliceous material, fly ash, and industrial waste [10].

***To whom all correspondence should be addressed.**

In recent years, the widespread utilization of synthetic dyes in various industrial sectors has led to growing concerns about their environmental impact. The discharge of dye-containing effluents into natural water bodies can result in adverse ecological consequences. Consequently, efficient and eco-friendly methods for the removal of these dyes from wastewater have garnered significant attention from researchers and environmentalists alike. Among the various approaches, adsorption has emerged as a promising technique due to its effectiveness in removing dyes from aqueous solutions [11]. Water contamination due to inadequate wastewater disposal practices by the textile industry has emerged as a formidable global challenge. Textile industries, serving as pivotal contributors to both the global economy and environmental degradation, have been implicated in widespread pollution concerns, notably within countries such as China and South Africa [12]. The effluents discharged by these industries, characterized by their profound coloration and the presence of persistent pollutants, bear a significant ecological burden, consequently affecting human health, an issue underscored [13, 14]. Evidently, the textile sector's immense role in this predicament is underscored by the annual production of approximately 7×10^7 tons of synthetic dyes globally, with a substantial portion—exceeding 10,000 tons—being utilized exclusively by textile operations [15]. A categorical classification of dyes based on origin, structure, and purpose is customary [16, 17]. Among these, the widespread application of dyes within the textile domain encompasses an array of types, including azo, direct, reactive, mordant, acid, basic, disperse, and sulfide dyes. In conjunction with the diverse spectrum of dye types, textile manufacturing involves an array of natural and synthetic fibers such as wool, cotton, silk, polyester, polyamide, and acrylic [18, 19]. The intricate stages of textile processing are frequently accompanied by the use of an assortment of chemical agents, which comprise sizing, softening, desizing, brightening, and finishing agents, many of which are notorious for their elevated toxicity levels [20]. Nonetheless, textile dyes exhibit limited affinity for fabric substrates, leading to their unbound release into aquatic ecosystems, including lakes, rivers, streams, and ponds, through wastewater discharges devoid of requisite treatment. This unregulated release constitutes a formidable ecological hazard, inflicting significant ecotoxicological ramifications characterized by detrimental impacts on various forms of aquatic life [21].

Nanotechnology holds the potential to revolutionize traditional approaches and pave the way for the advancement of next-generation wastewater treatment technologies, as supported by numerous studies [22-26]. In the realm of wastewater purification, the utilization of nanoparticles has gained prominence owing to their remarkable attributes, such as heightened reactivity, expansive surface area, versatile functionalization, and enhanced efficiency, as evidenced by multiple sources [27-32]. Within the spectrum of water treatment methodologies, adsorption stands out as a particularly effective technique due to its economical nature, heightened efficacy, and notable efficiency [33, 34].

In this context, the present study focuses on the use of boric acid zinc nanoalloys as a novel adsorbent for the removal of RB-5 dyestuff from aqueous solutions. RB-5 is a representative example of synthetic dyes commonly found in industrial effluents, and its effective removal is crucial for safeguarding aquatic ecosystems. The investigation delves into several key parameters that influence the adsorption process, including initial dyestuff concentration, solution pH, temperature, and equilibrium contact time. The interaction between RB-5 and boric acid zinc nanoalloys is examined through the application of various adsorption isotherm models, including Langmuir, Freundlich, DRK, and Temkin. These models provide valuable insights into the adsorption mechanisms and offer a comprehensive understanding of the equilibrium behavior of the adsorbate on the adsorbent surface. Of particular interest are the Langmuir and Temkin isotherms, which are found to adequately describe the adsorption process.

The study goes beyond isotherm and kinetic analyses by investigating the thermodynamic parameters associated with the RB-5 adsorption onto BA-Zn-nanoalloys. The determination of enthalpy, Gibbs free energy, and entropy changes provides valuable information about the spontaneity and endothermic nature of the adsorption process. Overall, the comprehensive investigation presented in this study contributes to the understanding of RB-5 dyestuff adsorption onto boric acid zinc nanoalloys, offering insights into the potential of this novel adsorbent for efficient and environmentally friendly dye removal from aqueous solutions. The findings not only advance the knowledge in the field of wastewater treatment but also pave the way for further exploration of advanced materials for sustainable environmental remediation.

Experimental

Preperation of Nano Zn/B(OH)3 Alloys

In this study Zn and B(OH)3 materials were used as received for the synthesis of nanoparticles. The

synthesis experiments were conducted by high energy planetary type ball (Retch PM100) by 250 ml hardened steel vial and 8-10 mm diameter balls. The milling processes were carried out for 30 hours at 350 rpm rotating speed. All sample handling and milling processes were carried under Argon atmosphere. The ball to powder ratio was selected as 20:1 The mill's direction of rotation was changed every 30 minutes and stopped for 10 minutes to increase the productivity and prevent the excessive e heat occurs during milling.

The crystal structure and morphological evolutions of the starting materials and milled alloys were followed by X-Ray Diffractometer (PanalyticalEmpryan) through CuK radiation at 45 kV and 40 mA and scanning electron microscopy (FEI Quanta FEG 450). The crystallite size and lattice strain of the alloys were defined by well-known Williamson-Hall technique [35].

Preparation of Dyestuff Solutions

To prepare the dyestuff solutions, stock solutions of 500-1000 mg/L (ppm) were prepared. Then, dye solutions at desired concentrations (10, 20, 30, and 40 mg/L) were obtained by dilution from the stock solutions. The pH of the dye solutions was adjusted in a pH meter (ISOLAB) using 0.1 M NaOH (Merk) and 0.1 M HCl (Merk) solutions.

Adsorption

Adsorption experiments were carried out in a temperature-controlled shaking water bath (Nüve ST 30) at 120 rpm stirring speed by adding 7 ml of dye solution on 0.04 g boric acid Zn nanoparticles. Then, at the determined time intervals (1, 10, 20, 30, 30, 60, 90, and 120 min), the samples in glass tubes were taken and centrifuged (Nüve CN 180) for 10 min at 3500 rpm. After centrifugation, the surface supernatants of the samples were removed. The maximum absorbance of these samples was measured in a UV-visible spectrophotometer (SHIMADZU UV-1800) at 597 nm for reactive black 5 at a maximum wavelength. The amount of dyestuff adsorbed on boric acid Zn nanoparticles was calculated by subtracting the initial concentration of the dye. The effect of parameters such as concentration, pH, temperature, and contact time on adsorption was investigated.

Calculation of the Amount of Dyestuff Removed in Solution Media

The following equation was used to calculate the amount of dyestuff removed from the solution medium.

$qe = (Co-Ce).v/w$

qe: Amount of adsorbed dyestuff per unit weight of adsorbent (mg/g).
Co : Initial concentration of dyestuff (mg/L).
Ce : Concentration of dyestuff remaining in the solution after adsorption (mg/L).
V: Volume of solution used (L).
W: Amount of adsorbent used (g).

Adsorption isotherm models

Freundlich isotherm

According to Freundlich, the adsorption sites on the surface of an adsorber are heterogeneous. They are composed of different types of adsorption sites. Freudlich, to explain adsorption from solution

He derived the equation $q_e : K_F.C_e^{1/n}$ [36].

In this equation, Ce: is the concentration of the substance remaining in the solution after adsorption ($mg.L^{-1}$), qe: is the amount of substance adsorbed on the unit adsorber ($mg.g^{-1}$), KF: is the adsorption capacity, n: adsorption density.

Taking the logarithm of both sides of the equation in the Freundlich isotherm equation. The expression $Logq_e=logK^F+1/nlogC_e$ is obtained. The Freundlich model is a model expressing adsorption on heterogeneous surfaces where the amount adsorbed at equilibrium increases as the pollutant concentration increases [37].

Langmuir isotherm

The adsorbed molecules form a saturated monolayer on the surface of the adsorber (Hameed, 2009). The Langmuir model is expressed by the following equation.

$1/qe=1/K_LQ_M.\ 1/Ce+1/Q_M$

Ce: concentration of the substance remaining in solution after adsorption ($mg.L^{-1}$), qe: amount of substance adsorbed per unit adsorber (($mg.g^{-1}$), KL: adsorbate-dependent constant (L/g), QM: monolayer adsorber capacity (mg/g).

To find the suitability of adsorption, the dimensionless constant RL is calculated. This constant is expected to take values between 0 and 1.

$R_L=1/1+K_LC_0$

Co is the initial concentration of the substance in solution [38].

Temkin isotherm

This isotherm takes into account the interactions between adsorbed substances and was developed by considering the heat of adsorption of all molecules in the solution [39].

Temkin equation $qe=RT/blna_T +RT/b.Ce$
If $RT/b=K_T$

The equation $qe= K_T \ln a_T +K_T.Ce$ is obtained.

a_T: Toth constant (L/g), T: temperature (K).

Dubinin-Radushkevich isotherm

The average adsorption energy calculated from the D-R isotherm gives information about the physical and chemical properties of adsorption [40]. The D-R isotherm is used to describe adsorption processes in the same type of porous structures. Mathematically

The equation $\ln qe= \ln Q_M-k.e^2$ is used [41].

Ce: concentration of the substance remaining in the solution after adsorption ($mg.L^{-1}$), qe: amount of substance adsorbed per unit adsorber ($mg.g^{-1}$), e: polany potential, k: D-R isotherm constant (e: epsilon).

Adsorption kinetics

Determining the kinetics of adsorption is important for the design of life-size systems for industrial applications. The kinetic study describes how fast the process occurs and the state of the factors affecting the reaction rate.

First order equations

The first order equations, also known as the Lagergren equation, is the equation that describes the adsorption rate for probabilistic liquid phase systems.

$dq/dt=k_1 .(qe-q)$
$\log(qe-q)= \log qe-k/2{,}303. T$

where qe (mg/g) is the amount of substance adsorbed at equilibrium and qt (mg/g) at any time t, k1 is the adsorption rate constant (min^{-1}).

Determining the qe value is the most difficult task. Because in many adsorbent-adsorbed interactions, adsorption occurs very slowly after a rapid onset. It is difficult to decide whether equilibrium is reached or not [42].

Quadratic equations

Second-order kinetic model
$dq/dt= k_2. (q_e-q)^2$
By taking the integral of this equation over the interval t=0 to t=t and qt=0, qt=qt

$t\ t/q =1/k_2.q^2_e +1/qe. T$
k2 is the adsorption rate constant (gmg/min), and qe is the amount of adsorbent at equilibrium (mg/g). The k2 quantity depends on the initial metal concentration, pH of the solution, temperature, and mixing ratio [43].

Intraparticle diffusion model

This model was developed by Weber and Morris
expressed by the equation $qt=k_i.t^{1/2} +C$.
k1 is the intraparticle diffusion rate constant ($mg/gdk^{0.5}$), C is constant. The rate constant ki is calculated from the slope of the graph of qt plotted against $t^{1/2.}$ C is the cut-off point.

Results and Discussion

Fig 1 depicts the XRD images of the starting materials and 30 milled nanoalloys. As seen clearly from the Fig 1, the crystalline peaks of the starting materials of the Zn (ICDD No: 87-0713, hexagonal, p63/mmc), ZnO (ICDD No: 89-0510, hexagonal, P63mc), B(OH)3 (ICDD No: 30-0199, triclinic, P-1) were observed without any undesired phases. When the XRD images of the 30 h milled samples are noticed, it can be seen that the phases of Zn4O(BO2)6 (ICDD No: 72-1316, cubic, I-43m) phases were observed after milling period together with minor unreacted Zn and ZnO. As seen, the whole amount of B(OH)3 were reacted with Zn/ZnO and formed a of Zn4O(BO2)6 phases. The crystallite size and lattice strain of the samples can be calculated commonly with Williamson-Hall Equations. The average crystallite size and lattice strain of the starting powders and milled samples are calculated as 68.2, 32 nm and %0.228 and %0.305 respectively. As expected, crystallite size were decreased as lattice strain decreased due to plastic deformations and impactions on lattice after milling procedures [44].

Fig 2 shows the SEM images of 30 h milled samples. The irregular shapes and morphologies were observed for the milled samples. These observations

can be seen in most of the studies conducted by ball milling methods [44-47]. As well known, the particles are continuously broken, then cold-weld after impactions between the balls and vials at the first stage of milling. With progressive of milling, particles are agglomerate and then breaks again. At the last stage of milling, particle size distribution and morphologies stay constant and observes in narrow range due to work-hardened mechanisms. After all, particle morphologies seems in irregular shapes [44].

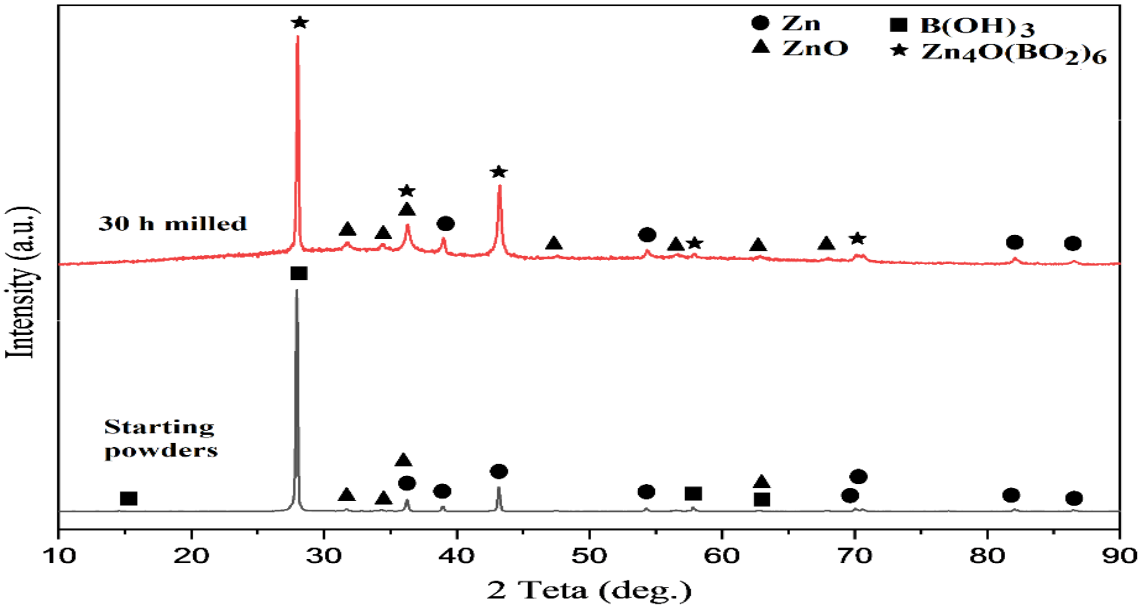

Fig. 1: XRD graphs of the starting materials and 30 h milled nanoalloys.

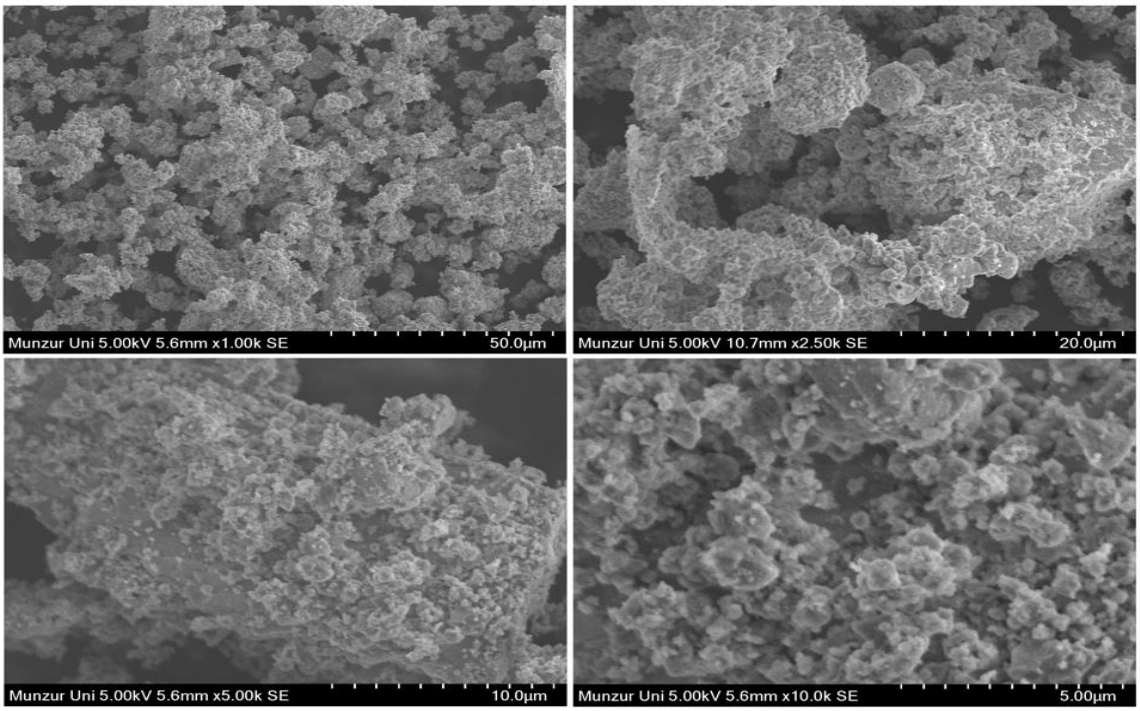

Fig. 2: SEM images of the 30 h milled nanoalloys.

Concentration Effect (25 ^{0}c)

Effect of Initial Dyestuff Concentration on Adsorption

To determine the effect of initial dyestuff concentration, reactive black-5 was studied at concentrations of 10, 20, 30 and 40 mg/L.

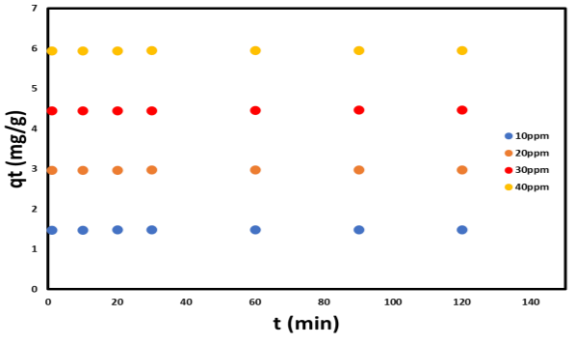

Fig. 3: Initial concentration of RB 5 adsorption on BA-Zn nanoparticles at 298K.

As seen in Fig 3, the adsorption behavior is similar at low concentrations and it reaches equilibrium as a result of high removal in very short periods of time, and after this point the amount of adsorbed dye does not change significantly. It was observed that at higher dye concentrations, the adsorption process was completed in longer periods of time. That is, adsorption was found to be significantly time and concentration dependent. For example; For a concentration of 20 mg/L, the maximum adsorption is 19.80 mg/g (99.02%) in the 20th minute, for 30 mg/L it is 29.68 mg/g (98.95%) in the 30th minute, 40 mg/g. The maximum adsorption for the L concentration was determined as 39.70 mg/g (98.26%) at the 120th minute. While it was observed that adsorption increased with increasing concentration, % adsorption decreased.

pH

The initial pH of dyestuff solutions causes changes in both the adsorbent and the amount of adsorbed dye. The effect of pH on RB-5 adsorption was carried out at three different pHs, 3, 7, and 11. Since RB-5 is generally anionic in solution, it tends to adsorb on positively charged solid surfaces.

It was observed that the decolorization rate was affected by the pH of the medium and decolorization was faster in acidic medium than in neutral and basic medium. The surface charge is positive since the H^+ ion concentration at pH 5 is high. This reduces adsorbent-adsorbate interaction. Increasing solution pH increases the number of OH^- groups and negatively charged sites.

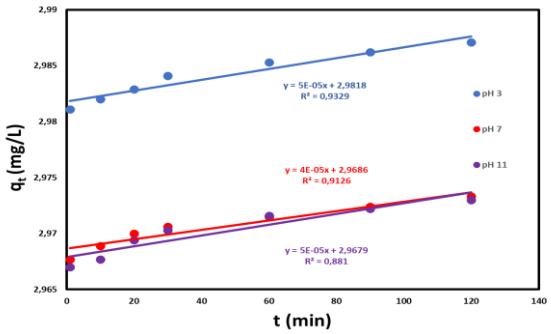

Fig. 4: Effect of pH on the adsorption of RB5 on the nanoparticle surface (C0=50mg/L, T=25°).

RB-5 is generally neutral and anionic in solution. It tends to adsorb on positively charged solid surface. Since RB-5 is an anionic dye, the electrostatic attraction forces of adsorbate and adsorbate are oppositely charged, so the adsorption of dye on the nanoparticle surface is higher in acid medium in Fig 4.

Effect of Temperature on Adsorption

The effect of temperature on adsorption was realized by experimental studies at 25°C, 35°C, 45°C, and 55°C. Fig 5 shows the effect of temperature on the adsorption of boric acid by Zn nanoparticles. As can be seen from the Fig, a high rate of adsorption was observed here from the first minutes and as time progressed, the adsorption reached its maximum level and the maximum adsorption was 19.84 mg/g (99.40%) in the 120th minute at 250C, maximum adsorption at 350C, 450C and 550C, respectively. It was determined as 19.91 mg/g (99.59%), 19.93 mg/g (99.66%) and 19.95 mg/g (99.76%). Since the adsorbed amounts are very close to each other according to temperatures, the effect of temperature is low. The increase in adsorption capacity with increasing temperature, albeit slightly, indicates that the adsorption phenomenon is endothermic.

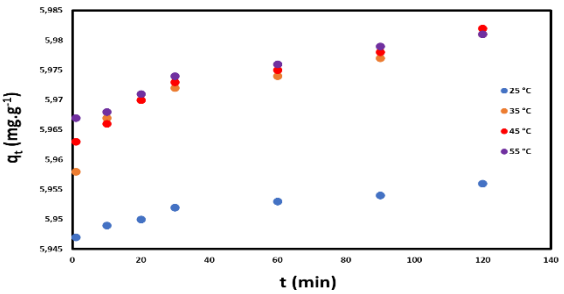

Fig. 5: Temperature effect of RB5 at a concentration of 50 mg/L on nanoparticles (pH: 8.24, W/V: 0.04 g).

Isotherm studies

Freundlich Adsorption Isotherm

Freundlich Equation

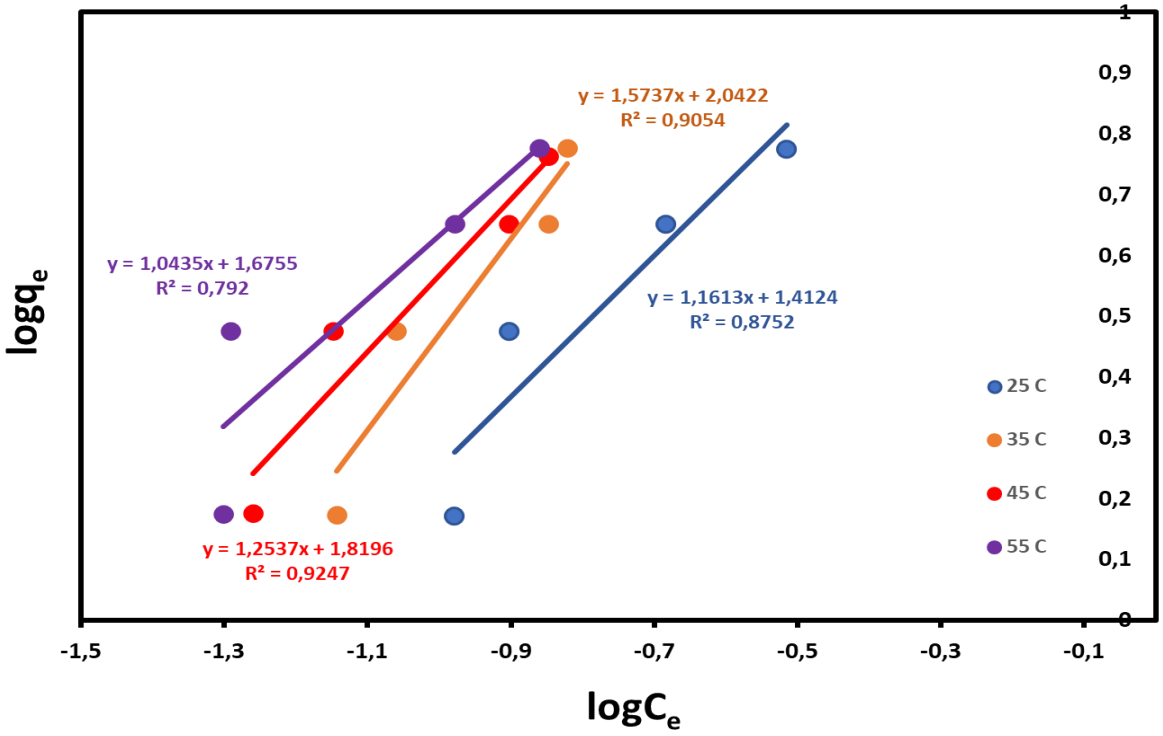

Fig. 6: Freundlich isotherm of adsorption of RB-5 on nanoparticles.

T(K)	:	298	308	318	328
K_F (mg.g^{-1})	:	0,1499	0,3100	0,2599	0,2241
n	:	0,8611	0,6354	0,7976	0,9583
R^2	:	0,8752	0,9054	0,9247	0,792

Freundlich isotherms were evaluated according to the correlation coefficient (R^2) results. It is known that when the correlation coefficient approaches 1, the suitability increases. When the adsorption intensity (n) takes a value between 1 and 10, it indicates that the adsorption process is suitable.

Here, the KF value, which expresses the adsorption capacity, is 0.1449 at 25^{0}C, 0.3100 at 35^{0}C, 0.2599 at 45^{0}C and 0.2241 at 55^{0}C, respectively, and the value of n, which expresses the adsorption intensity, for the same temperatures, respectively. It was found to be 0.8611, 0.6354, 0.7976 and 0.9583 in Fig 6.

It was determined that the correlation values for RB-5 at 45 ^{0}C were 0.9247 and lower for other temperatures. The adsorption of RB-5 by BA-Zn-nanoalloys was found to be partially compliant at 35 ^{0}C and 45 ^{0}C. At different temperatures, it was observed that it did not fit the Freundlich isotherm due to low correlation values. The reason for the Freundlich isotherm graph in the 4th region is that the adsorption occurs at low concentrations (Fig 6).

Langmuir Izoterm Modeli

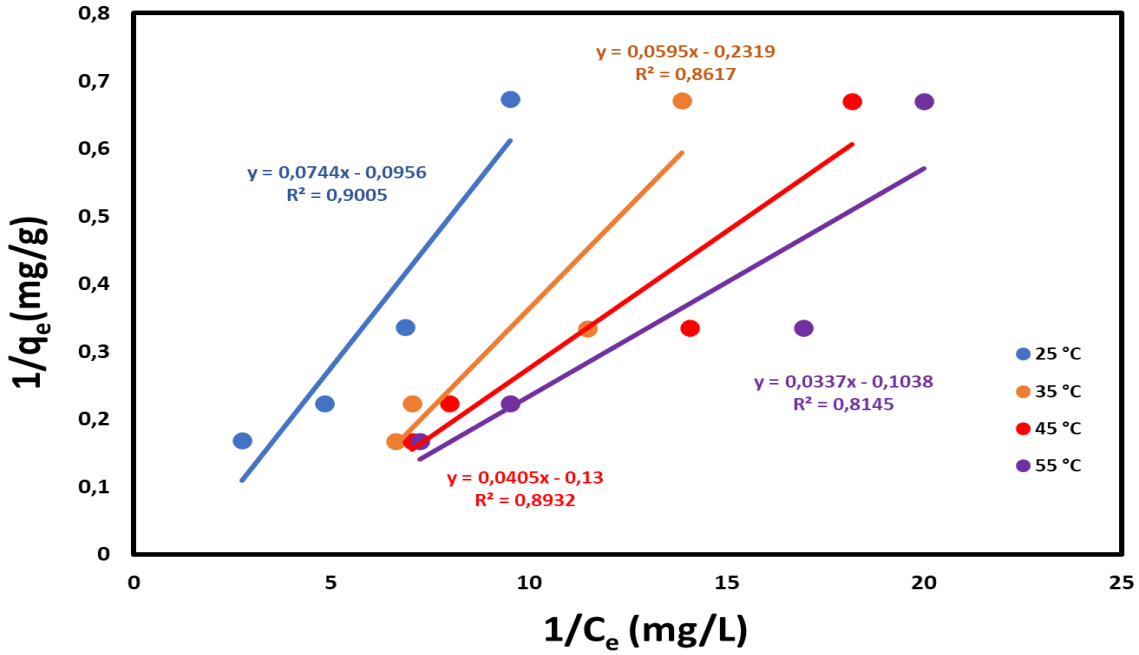

Fig. 7: Langmuir isotherm of adsorption of RB-5 on nanoparticles.

Langmuir isotherm constants for adsorption of RB-5 on boric acid Zn nanoparticles at different temperatures. Langmuir isotherms drawn on BA-Zn nanoalloys at different temperatures without changing the pH of the RB 5 dye are shown in Fig 7. As seen in the table, since the correlation values for RB 5 at different temperatures are high, it can be said that the adsorption fits the Langmuir isotherm model. Accordingly, the adsorption of the dyestuff occurs in specific homogeneous regions on the nanoparticle, and also that the dyestuff is covered as a monolayer on the boric acid Zn surface. Qm, which expresses the Langmuir adsorption capacity for RB 5, is 11.77 mg/g at 250C, 19.19 mg/g at 350C, 28.49 mg/g at 450C and 23.58 mg/g at 550C. has been calculated. The b values expressing the adsorption energy were found to be 0.59 L/mg, 0.85 L/mg, 0.69 L/mg and 0.18 L/mg for the same temperatures, respectively. As can be seen from the table, all RL values are between 0 and 1, which shows that the adsorption for the dyestuff occurs harmoniously.

T (K)	298	308	318	328
b (L/mg)	0,5970	0,8598	7,69	0,1865
qm (mg.g)	11,77	19,19	28,49	23,58
R^2	0,9848	0,9919	0,9723	0,9633
R_L	0,052	0,037	0,1150	0,1517

Since the correlation values for RB-5 were high, it fit the Langmuir isotherm model in Fig 5. Accordingly, boric acid for RB-5 was realized in homogeneous regions on zinc nanoparticles. Also, RB-5 was covered as a single layer on the nanoparticle surface.

The graphs obtained by applying the Temkin isotherm derived by considering the interactions between the adsorbed species and the adsorbent to the adsorption data of RB 5 by boric acid Zn nanoparticle using the equation qe=KT lnaT +KT.Ce are given in Fig 8. Temkin isotherm equilibrium binding constant AT and B=RT/bT values known as heat of adsorption and correlation values are presented in the Table. Considering the correlation values obtained for the dyestuff, it can be said that there is compliance with Temkin. According to this, the heat of adsorption of all molecules in the layer for RB 5 decreases linearly as the surface is covered due to adsorbent and adsorbate interactions.

Temkin isotherm model

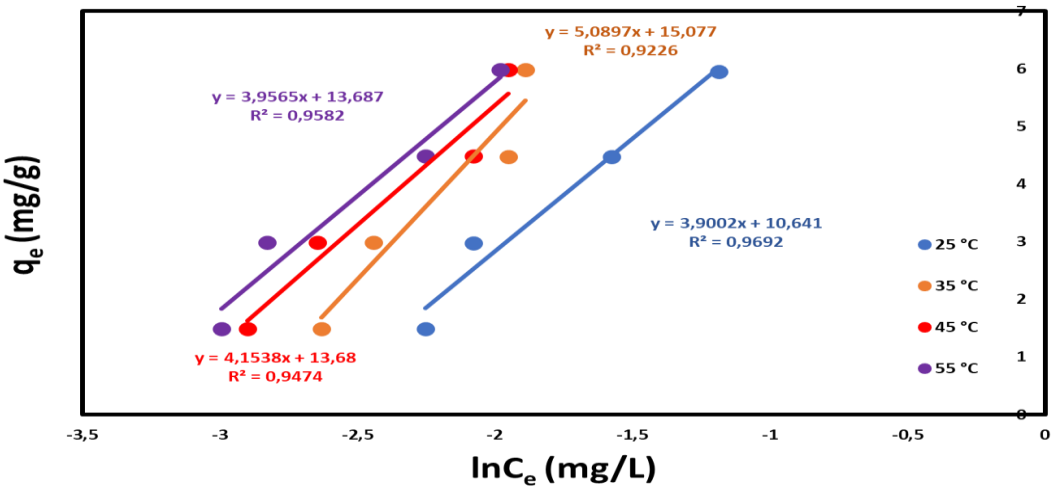

Fig 8. Temkin isotherm for adsorption of RB-in on nanoparticles

T(K)	**298**	**308**	**318**	**328**
b_T	635	503	616	689
A_T	1,003	1,08	1,19	1,24
R^2	0,9692	0,9226	0,9474	0,9582

DRK isotherm model

DRK 298K (10ppm 20ppm 30ppm 40ppm).

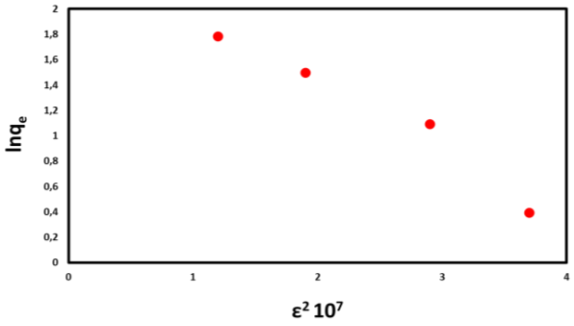

Fig. 9: DR isotherm curve of RB 5 adsorption on nanoparticles(298K).

lnq_e	**E^2 (epsilon)**
0,3948	$3,7.10^7$
1,0923	$2,9.10^7$
1,4971	$1,9.10^7$
1,7840	$1,2.10^7$

y= -1,5702x+4,2218
R^2= 0,9165
E=1,77

The adsorption energy (E) obtained from the D-R adsorption isotherm is 1.09 kj.mol^{-1}. The fact that this value is less than 8 kjmol^{-1} indicates that adsorption is related to physical interactions in Fig 9.

Pseudo First Order Kinetic Model

Table-1: Pseudo-first order kinetic parameters of RB-5 at different concentrations on nanoparticles (298 K).

Concentration	Experimental q_e mg.g^{-1}	k_1(dk^{-1})	calculated q_e	R^2
10	1,484	0,0237	3,770	0,9993
20	2,981	0,0237	0,014	0,995
30	4,478	0,0110	0,220	0,9907
40	5,954	0,0170	0,272	0,6936

Considering the correlation values in the table, the correlation values are low, it can be said that the adsorption does not fit the pseudo-first order kinetic model (Table 1). In addition, even if the correlation values of the graphs belonging to the pseudo-first order kinetic model are high, the q_e values obtained from the equations should be the same or

very close to each other with the experimental q_e in order to be able to talk about compliance with this model. Here, no agreement was observed in q_e values (Fig 10).

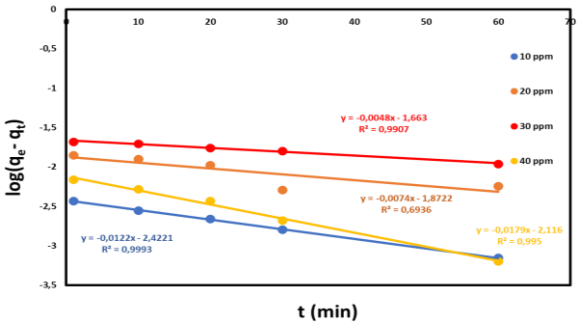

Fig. 10: Pseudo-first order kinetic graph of adsorption of different concentrations of RB-5 on nanoparticles (T: 298 K).

Pseudo Second-Order Kinetic Model

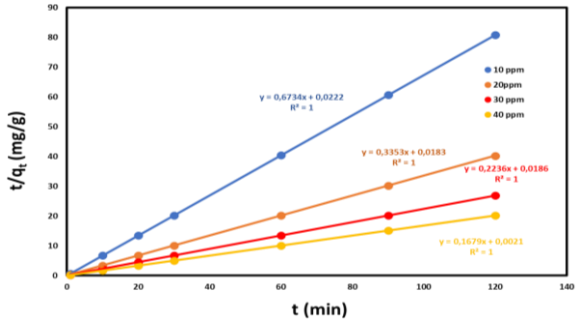

Fig. 11: Pseudo-second order kinetic graph of adsorption of RB-5 on nanoparticles at different concentrations (T: 298 K).

qe (mg/g)	1,4852	2,9824	4,4722
5,9542			
experimental qe (mg/g)	1,4842	2,9812	4,4689
5,9542			
R^2	1	1	1
1			
k_2	24,39	8,58	4,037
94,93			

It is seen that the correlation values of the graphs obtained for the dyestuff are 1. In addition, the fact that the qe values obtained from the equations are very close to the experimental qe values, it is said that the adsorption fits the pseudo-second-order kinetic model. This indicates that there may be a chemical interaction between the RB-5 dyestuff and the nanoparticle (Fig 11).

Intra-Particulate Diffusion Model

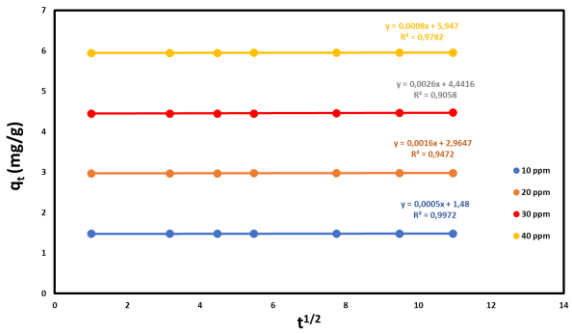

Fig. 12: Graph of intraparticle diffusion kinetics of adsorption of different concentrations of RB-5 on nanoparticles.

Upon analyzing the intraparticle diffusion line in Fig 12, it becomes evident that the resultant lines exhibit diffraction. Each line has two linear areas. These findings indicate that the adsorption process has several distinct steps. Due to the porous nature of the adsorbent utilized in adsorption, pore diffusion is anticipated in addition to surface adsorption.

Concentration (mg/L)	**k_i**	**R^2**
10		0,0005
0,9972		
20		0,0016
0,9472		
30		0,0025
0,8738		
40		0,0080
0,9662		

Thermodynamic parameters related to adsorption

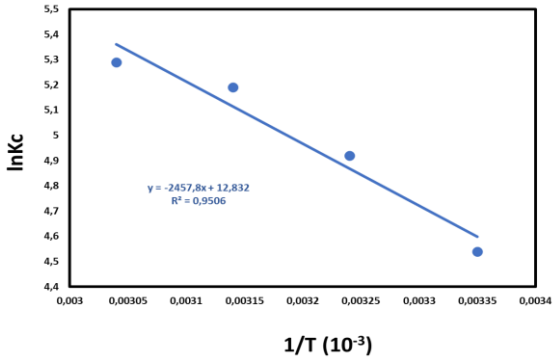

Fig. 13: Thermodynamic graph of RB5 adsorption of nanoparticle.

Temperature (C^0)	lnKc	ΔG^0 j/mol		ΔH^0 j/mol	ΔS^0 j/mol.K
25	4,54	-11248,17			
35	4,92	-12598,70	20,43	106,68	
45	5,19	-13721,59			
55	5,29	-14425,78			

Thermodynamic calculations of the adsorption of RB 5 dye onto BA-Zn nanoparticles were carried out at 10 mg/L dye concentration and natural pH values at temperatures of 25, 35, 45, and 55°C. The ΔGº, ΔHº, and ΔSº values obtained as a function of temperature are given in the table. The table shows that the ΔGº values for RB 5 dyestuff were negative. The adsorption of RB 5 by the nanoparticle is a spontaneous process. For RB 5, the negative value of ΔGº goes down as the temperature rises, and the nanoparticles are better able to adsorb RB 5 on their own when the temperature is higher. The standard enthalpy (ΔHº) and standard entropy (ΔSº) values of RB 5 were found to be positive. A positive ΔHº value indicates that adsorption occurs endothermally, and a positive ΔSº value indicates that there may be some structural changes on the adsorbent surface. Low ΔSº values for the dyestuff indicate that non-significant changes in entropy have occurred. Fig 13 indicates that the adsorption of the dyestuff by the nanoparticle is a spontaneous process. ΔG^0 decreases with increasing temperature. The standard enthalpy and standard entropy values were positive. A positive enthalpy indicates that adsorption is exothermic. A positive ΔS^0 value indicates that there are some changes on the adsorbent surface. The low ΔS^0 value for RB-5 indicates that there is no significant change in entropy.

The research of RB-5 dyestuff adsorption onto boric acid-zinc nanoalloys is intriguing, since it involves investigating isotherm, kinetic, and thermodynamic features. The examination of isotherms, using the Langmuir, Freundlich, and Temkin models, help to understand the characteristics of adsorption. Meanwhile, kinetic studies that apply pseudo-first-order and pseudo-second-order models offer valuable information about the step that limits the pace of the process. Thermodynamic analyses, which involve the determination of parameters such as Gibbs free energy change (ΔG°), enthalpy change (ΔH°), and entropy change (ΔS°), provide insights on the spontaneity and energy changes associated with the process.

Dalvand and groups (48) investigated the efficacy of Fe_3O_4 magnetic nanoparticles functionalized with amine groups and containing L-arginine (Fe_3O_4@L-arginine) for the removal of RB5 azo dye from water. The tests were formulated utilizing the Box-Behnken design methodology to optimize the adsorption parameters. Fe_3O_4@L-arginine nanoparticles were successfully produced. The most effective conditions for dye adsorption were a dye concentration of 50 mg/L, an adsorbed dosage of 0.8 g/L, and a pH of 3. These parameters resulted in an efficiency of 97.6%, which closely matched the model's predicted efficiency of 96.8%, thereby proving the validity of the model. The adsorption of RB5 dye followed the pseudo-second-order kinetic and Temkin isotherm models, which means it was a heat-absorbing and thermodynamically favorable process. The study discovered that Fe_3O_4@L-arginine nanoparticles have a high capacity for adsorbing RB5 dye, exhibiting efficient adsorption capabilities throughout multiple cycles. Fe_3O_4@L-arginine nanoparticles are highly effective in eliminating dye from wastewater due to their exceptional performance, convenient production and application, and effortless separation. Sutlovic and colleagues (49) was to investigate the impact of the initial pH (pH_0) on the isothermal adsorption of Reactive Black 5 (RB5) dye on commercially available activated carbon. The experiment employed pH values of 2.00, 4.00, 8.00, and 10.00. The adsorption kinetics mechanism has been investigated through the utilization of pseudo-first-order, pseudo-second-order, and intraparticle diffusion models. Furthermore, the thermodynamic properties of adsorption were determined using a pH_0 value of 4.00. The findings of this investigation indicate that the initial pH level has a significant impact on the adsorption of RB5 dye on activated carbon. The highest adsorption capacities (qe) and decoloration efficiencies were seen at pH_0 = 2.00 (q_e = 246.0 mg g^{-1}) and 10.00 (q_e = 239.1 mg g^{-1}), respectively, due to the presence of robust electrostatic and attractive π···π interactions. The study showcased the ability to manipulate the rate of RB5 dye adsorption on activated carbon across all pH levels through kinetic control, employing a pseudo-second-order model. The adsorption rate was not exclusively determined by intraparticle diffusion. Sobrinho and team (50) worked that Diethylenetriamine in the Hummers process produced nGO-(NH)R, a multi-layered amino-functionalized graphene oxide. X-ray diffraction, scanning electron microscopy, atomic force microscopy, thermogravimetric analysis, Raman, infrared, and nGO-(NH)R analysis were used. Reactive Black 5 (RB5) and methylene blue were absorbed. At pH 12.0, cationic MB adsorption increased, whereas anionic RB5 did not. The Langmuir isotherm efficiently adsorbs both dyes onto nGO-(NH)R, with MB and RB5 obtaining 3036.43 and 335.86 mg g^{-1} monolayer adsorption capacities,

respectively. MB and RB5 adsorption kinetics were examined. MB reached equilibrium in 5 minutes, but RB5 took 90. The equilibrium adsorption capacity (q_e) for MB was 977.06 mg g^{-1} with a rate constant (k_S) of 3.17×10−2 g mg−1 min. The equilibrium adsorption capacity (qe) of RB5 was not supplied; however, the rate constant (k_S) was determined at 2.40×10^{-3} g mg^{-1} min. Additionally, the pseudo-second-order model better matched nGO and nGO-(NH)R dye adsorption experiments. Adsorption and chemisorption of MB and RB5 on nGO-(NH)R showed spontaneous behavior, with ΔH^o = -150.01 kJ mol^{-1} and ΔG^o = -37.94 and -22.86 at 298 K.

The findings from these investigations contribute collectively to a full comprehension of the RB-5 adsorption onto boric acid-zinc nanoalloys, providing vital insights for enhancing the effectiveness of this system in possible applications, especially in wastewater treatment.

Conclusion

In this study, the adsorption of RB-5 dyestuff on the boric acid zinc nanoparticle surface was investigated. The effect of solution concentration, contact time, pH, and temperature on the removal of the dye from aqueous media was investigated.

At low concentrations, the adsorption process reaches the equilibrium state faster due to the low ratio of dye molecules to adsorption sites. An increase in adsorption was observed with increasing initial dye concentration. Another factor on which the adsorption process depends is the contact time. Because the equilibrium time of each sample is different. The adsorption of RB-5 was investigated over a period of 1 to 120 minutes. Up to 90 minutes adsorption was observed to increase. After that, no significant increase was observed and the adsorption rate remained constant. Therefore, the dye removal rate for RB-5 was determined as 90 min. The experimental data were analyzed for Langmuir, Freundlich, Temkin, and Dubinin-Radushkevich isotherms. The most suitable isotherms were found to be Langmuir and Temkin. The adsorption energy obtained from DR adsorption isotherm is 1.08 kj/mol. This is an indication that adsorption is related to physical interactions. pH is a parameter that affects not only the adsorbent properties but also the nanoparticle surface structure. This factor was studied by evaluating the dye removal capacity of adsorbent samples at different pHs from 3 to 11. Increasing the pH from 3 to 11 resulted in an increase in the percentage of adsorption. According to kinetic investigations, the process was found to fit a pseudo-second-order kinetic model. Thermodynamic analysis showed that the process was exothermic, spontaneous, and physical adsorption.

In conclusion, the nanoparticle used in this study was found to be a suitable adsorbent for RB-5 adsorption and can be used as an alternative adsorbent for the adsorption of other dyes.

References:

1. El Bouraie, M. and W.S. El Din, *Biodegradation of Reactive Black 5 by Aeromonas hydrophila strain isolated from dye-contaminated textile wastewater.* Sustainable Environment Research, 2016. **26**(5): p. 209-216.
2. Chequer, F.M.D., D.J. Dorta, and D.P. de Oliveira, *Azo dyes and their metabolites: does the discharge of the azo dye into water bodies represent human and ecological risks.* Advances in treating textile effluent, 2011. **48**: p. 28-48.
3. Vakili, M., et al., *Application of chitosan and its derivatives as adsorbents for dye removal from water and wastewater: A review.* Carbohydrate polymers, 2014. **113**: p. 115-130.
4. Zainudin, N.S., M. Yaacoba, and Z. Othman, *Stability of reactive black 5 (RB5) standard solution studied in different conditions.* Health and the Environment Journal, 2016. **7**(1): p. 87-100.
5. Kim, T.-H., et al., *Comparison of disperse and reactive dye removals by chemical coagulation and Fenton oxidation.* Journal of hazardous materials, 2004. **112**(1-2): p. 95-103.
6. Zhu, Z., et al., *Effect of polymeric matrix on the adsorption of reactive dye by anion-exchange resins.* Journal of the Taiwan Institute of Chemical Engineers, 2016. **62**: p. 98-103.
7. Amin, M.T., A.A. Alazba, and M. Shafiq, *Adsorptive removal of reactive black 5 from wastewater using bentonite clay: isotherms, kinetics and thermodynamics.* Sustainability, 2015. **7**(11): p. 15302-15318.
8. Al-Momani, F., et al., *Biodegradability enhancement of textile dyes and textile wastewater by VUV photolysis.* Journal of photochemistry and Photobiology A: Chemistry, 2002. **153**(1-3): p. 191-197.
9. Xiong, W., et al., *Adsorption of phosphate from aqueous solution using iron-zirconium modified activated carbon nanofiber: performance and mechanism.* Journal of colloid and interface science, 2017. **493**: p. 17-23.
10. Talwar, K., et al., *Statistical analysis of acid blue-113 dye removal using palm tree male flower activated carbon.* Int J Appl Environ Sci, 2016. **11**(2): p. 475-490.

11. Amin, M., A. Alazba, and M. Shafiq, *LDH of NiZnFe and its composites with carbon nanotubes and data-palm biochar with efficient adsorption capacity for RB5 dye from aqueous solutions: Isotherm, kinetic, and thermodynamics studies.* Current Applied Physics, 2022. **40**: p. 90-100.
12. Olisah, C., J.B. Adams, and G. Rubidge, *The state of persistent organic pollutants in South African estuaries: A review of environmental exposure and sources.* Ecotoxicology and Environmental Safety, 2021. **219**: p. 112316.
13. Almroth, B.C., et al., *Assessing the effects of textile leachates in fish using multiple testing methods: From gene expression to behavior.* Ecotoxicology and Environmental Safety, 2021. **207**: p. 111523.
14. Ali, S.S., R. Al-Tohamy, and J. Sun, *Performance of Meyerozyma caribbica as a novel manganese peroxidase-producing yeast inhabiting wood-feeding termite gut symbionts for azo dye decolorization and detoxification.* Science of The Total Environment, 2022. **806**: p. 150665.
15. Chandanshive, V., et al., *In situ textile wastewater treatment in high rate transpiration system furrows planted with aquatic macrophytes and floating phytobeds.* Chemosphere, 2020. **252**: p. 126513.
16. Akpomie, K.G. and J. Conradie, *Advances in application of cotton-based adsorbents for heavy metals trapping, surface modifications and future perspectives.* Ecotoxicology and Environmental Safety, 2020. **201**: p. 110825.
17. Holkar, C.R., et al., *A critical review on textile wastewater treatments: possible approaches.* Journal of environmental management, 2016. **182**: p. 351-366.
18. Deopura, B. and N. Padaki, *Synthetic textile fibres: polyamide, polyester and aramid fibres*, in *Textiles and Fashion*. 2015, Elsevier. p. 97-114.
19. Silva, A.C., et al., *Modification of textiles for functional applications*, in *Fundamentals of natural fibres and textiles*. 2021, Elsevier. p. 303-365.
20. Kishor, R., et al., *Ecotoxicological and health concerns of persistent coloring pollutants of textile industry wastewater and treatment approaches for environmental safety.* Journal of Environmental Chemical Engineering, 2021. **9**(2): p. 105012.
21. Parmar, S., et al., *Microorganism: An ecofriendly tool for waste management and environmental safety*, in *Development in Wastewater Treatment Research and Processes*. 2022, Elsevier. p. 175-193.
22. Zafar, M.N., et al., *Effective adsorptive removal of azo dyes over spherical ZnO nanoparticles.* Journal of Materials Research and Technology, 2019. **8**(1): p. 713-725.
23. Rahmat, M., et al., *Highly efficient removal of crystal violet dye from water by MnO2 based nanofibrous mesh/photocatalytic process.* Journal of Materials Research and Technology, 2019. **8**(6): p. 5149-5159.
24. Jamil, A., et al., *Photocatalytic degradation of disperse dye Violet-26 using TiO2 and ZnO nanomaterials and process variable optimization.* Journal of Materials Research and Technology, 2020. **9**(1): p. 1119-1128.
25. Bibi, I., et al., *Green synthesis of iron oxide nanoparticles using pomegranate seeds extract and photocatalytic activity evaluation for the degradation of textile dye.* Journal of Materials Research and Technology, 2019. **8**(6): p. 6115-6124.
26. Ajmal, S., et al., *Effect of Fe and Bi doping on LaCoO3 structural, magnetic, electric and catalytic properties.* Journal of Materials Research and Technology, 2019. **8**(5): p. 4831-4842.
27. Fu, Y., et al., *Au nanoparticles decorated on activated coke via a facile preparation for efficient catalytic reduction of nitrophenols and azo dyes.* Applied Surface Science, 2019. **473**: p. 578-588.
28. Fu, Y., et al., *Chitosan functionalized activated coke for Au nanoparticles anchoring: Green synthesis and catalytic activities in hydrogenation of nitrophenols and azo dyes.* Applied Catalysis B: Environmental, 2019. **255**: p. 117740.
29. Qin, L., et al., *Hierarchical porous carbon material restricted Au catalyst for highly catalytic reduction of nitroaromatics.* Journal of hazardous materials, 2019. **380**: p. 120864.
30. Wang, W., et al., *Sulfur doped carbon quantum dots loaded hollow tubular g-C3N4 as novel photocatalyst for destruction of Escherichia coli and tetracycline degradation under visible light.* Chemical Engineering Journal, 2019. **378**: p. 122132.
31. Zhan, F., et al., *Facile preparation and highly efficient catalytic performances of Pd-Cu bimetallic catalyst synthesized via Seed-mediated method.* Nanomaterials, 2019. **10**(1): p. 6.
32. Zhao, J., et al., *Facile preparation of a self-assembled artemia cyst shell–TiO2–MoS2 porous composite structure with highly efficient catalytic reduction of nitro compounds for wastewater treatment.* Nanotechnology, 2019. **31**(8): p. 085603.
33. Sohail, I., et al., *Polyamidoamine (PAMAM) dendrimers synthesis, characterization and adsorptive removal of nickel ions from aqueous*

solution. Journal of Materials Research and Technology, 2020. **9**(1): p. 498-506.
34. Bhatti, H.N., et al., *Biocomposite application for the phosphate ions removal in aqueous medium.* Journal of Materials Research and Technology, 2018. **7**(3): p. 300-307.
35. Williamson, G. and W. Hall, *X-ray line broadening from filed aluminium and wolfram.* Acta metallurgica, 1953. **1**(1): p. 22-31.
36. Freundlich, H. and H. Hatfield, *Colloid and capillary chemistry, Methuen and Co.* Ltd., London, 1926: p. 110-114.
37. Wise, D.L. and D.J. Trantolo, *Remediation of hazardous waste contaminated soils.* (No Title), 1995.
38. Weber, T.W. and R.K. Chakravorti, *Pore and solid diffusion models for fixed-bed adsorbers.* AIChE Journal, 1974. **20**(2): p. 228-238.
39. Temkin, M. and V. Pyzhev, *Recent modifications to Langmuir isotherms.* 1940.
40. Dąbrowski, A., *Adsorption—from theory to practice.* Advances in colloid and interface science, 2001. **93**(1-3): p. 135-224.
41. Ho, Y.-S., *Absorption of heavy metals from waste streams by peat*. 1995, University of Birmingham.
42. Doğan, M. and M. Alkan, *Adsorption kinetics of methyl violet onto perlite.* Chemosphere, 2003. **50**(4): p. 517-528.
43. Ho, Y.-S. and G. McKay, *Pseudo-second order model for sorption processes.* Process biochemistry, 1999. **34**(5): p. 451-465.
44. Suryanarayana, C., *Mechanical alloying and milling.* Progress in materials science, 2001. **46**(1-2): p. 1-184.
45. Karimi, L., et al., *Improvement of magnetic properties of nanostructured Ni79Fe16Mo5 alloyed powders by a suitable heat treatment.* Advanced Powder Technology, 2013. **24**(3): p. 653-658.
46. Slimi, M., et al., *Structural and microstructural properties of nanocrystalline Cu–Fe–Ni powders produced by mechanical alloying.* Powder technology, 2014. **266**: p. 262-267.
47. Abbasi, S., H. Eslamizadeh, and H. Raanaei, *Study of synthesis, structural and magnetic properties of nanostructured (Fe67 Ni33) 70 Ti10 B20 alloy.* Journal of Magnetism and Magnetic Materials, 2018. **451**: p. 780-786.
48. Pormazar, S. M., & Dalvand, A. (2022). Adsorption of Reactive Black 5 azo dye from aqueous solution by using amine-functioned Fe3O4 nanoparticles with L-arginine: Process optimisation using RSM. *International Journal of Environmental Analytical Chemistry*, *102*(8), 1764-1783.
49. Vojnović, B., Cetina, M., Franjković, P., & Sutlović, A. (2022). Influence of initial pH value on the adsorption of reactive black 5 dye on powdered activated carbon: Kinetics, mechanisms, and thermodynamics. *Molecules*, *27*(4), 1349.
50. Fraga, T. J. M., De Souza, Z. S. B., Marques Fraga, D. M. D. S., Carvalho, M. N., de Luna Freire, E. M. P., Ghislandi, M. G., & da Motta Sobrinho, M. A. (2020). Comparative approach towards the adsorption of Reactive Black 5 and methylene blue by n-layer graphene oxide and its amino-functionalized
derivative. *Adsorption*, *26*(2), 283-301.